END
DATE
FILMED
10-81
DTIC

Impedance and Mass Transport Kinetics of Nickel Cadmium Cells

Prepared by

A. H. ZIMMERMAN and M. C. JANECKI
Chemistry and Physics Laboratory
Laboratory Operations
The Aerospace Corporation
El Segundo, Calif. 90245

1 September 1981
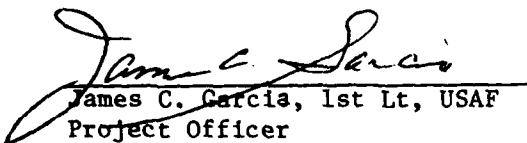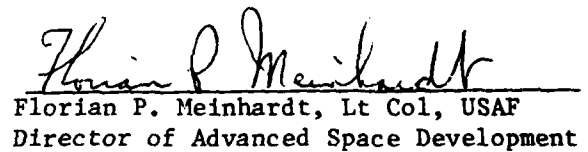
This report was submitted by The Aerospace Corporation, El Segundo, CA 90245, under Contract No. F04701-80-C-0081 with the Space Division, P.O. Box 92960, Worldway Postal Center, Los Angeles, CA 90009. It was reviewed and approved for The Aerospace Corporation by S. Feuerstein, Director, Chemistry and Physics Laboratory. Lt James C. Garcia, SD/YLVS, was the project officer for Mission-Oriented Investigation and Experimentation (MOIE) Programs.
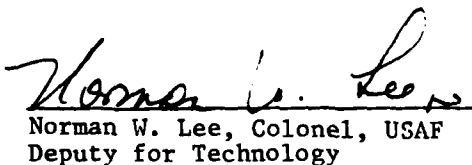
This report has been reviewed by the Public Affairs Office (PAS) and is releasable to the National Technical Information Service (NTIS). At NTIS, it will be available to the general public, including foreign nations.

This technical report has been reviewed and is approved for publication. Publication of this report does not constitute Air Force approval of the report's findings or conclusions. It is published only for the exchange and stimulation of ideas.

James C. Garcia, 1st Lt, USAF
Project Officer

Florian P. Meinhardt, Lt Col, USAF
Director of Advanced Space Development

FOR THE COMMANDER

Norman W. Lee, Colonel, USAF
Deputy for Technology

REPORT DOCUMENTATION PAGE		READ INSTRUCTIONS BEFORE COMPLETING FORM
1. REPORT NUMBER SD-TR-81-63	2. GOVT ACCESSION NO. AD-A105 320	3. RECIPIENT'S CATALOG NUMBER
4. TITLE (and Subtitle) IMPEDANCE AND MASS TRANSPORT KINETICS OF NICKEL CADMIUM CELLS		5. TYPE OF REPORT & PERIOD COVERED
		6. PERFORMING ORG. REPORT NUMBER TR-0081(6970-01)-1
7. AUTHOR(s) Albert H. Zimmerman and Melanie C. Janecki		8. CONTRACT OR GRANT NUMBER(s) F04701-80-C-0081
9. PERFORMING ORGANIZATION NAME AND ADDRESS The Aerospace Corporation El Segundo, Calif. 90245		10. PROGRAM ELEMENT, PROJECT, TASK AREA & WORK UNIT NUMBERS
11. CONTROLLING OFFICE NAME AND ADDRESS Space Division Air Force Systems Command Los Angeles, Calif. 90009		12. REPORT DATE 1 September 1981
		13. NUMBER OF PAGES 27
14. MONITORING AGENCY NAME & ADDRESS(if different from Controlling Office)		15. SECURITY CLASS. (of this report) Unclassified
		15a. DECLASSIFICATION/DOWNGRADING SCHEDULE

16. DISTRIBUTION STATEMENT (of this Report)

Approved for public release; distribution unlimited.

17. DISTRIBUTION STATEMENT (of the abstract entered in Block 20, if different from Report)

18. SUPPLEMENTARY NOTES

19. KEY WORDS (Continue on reverse side if necessary and identify by block number)

Battery
Diffusion
Electrolyte
Impedance

20. ABSTRACT (Continue on reverse side if necessary and identify by block number)

The impedance of operating NiCd cells in the frequency range 0.001 to 100 Hz is characteristic of mass-transport processes that occur in the cells. Two diffusion processes are observed in the impedance spectrum, at least one of which appears to involve solid-state diffusion in a surface film. The diffusion characteristics have a pronounced dependence on cell current, as well as some dependence on cell state-of-charge and operating temperature. The diffusion properties of the NiCd cell do appear to be sensitive to the changes in morphological or chemical structure of the active materials that can occur during use.

DD FORM 1473
(FACSIMILE)

CONTENTS

FIGURES

3

I. INTRODUCTION

The impedance properties of battery cells provide a useful and nondestructive means for characterizing the processes that occur in a battery cell during both operating and open-circuit conditions. Most of the impedance measurements previously reported have been in the audio frequency range and have been primarily concerned with either an electrical characterization of the cell or a state-of-charge monitor based on the cell impedance properties. Impedance measurements reported by Brodd and DeWane[1] indicate an inductive impedance for sealed NiCd cells at frequencies above several kilohertz. This phenomenon has been observed for other battery cells[2] and is generally attributed to inductances arising from the physical structure of the internal cell conductors. Measurements of NiCd cell impedances at a fixed frequency,[3] typically 1000 Hz, indicate a decreasing cell impedance as cell capacity or size increases. Lurie et al.[4] reported the alternating current impedance of 20-Ah NiCd cells in the frequency range 1 Hz to 100 kHz as part of their effort to devise a state-of-charge indicator for NiCd batteries. They concluded that the cell impedance was most sensitive to state of charge at the lowest frequencies. Recently, Sathyanarayana et al.[5] reported detailed measurements of the impedance of open-circuit NiCd cells between 5 and 30 Hz. These measurements were obtained in an experimental study of the relationships between the impedance properties of a cell and its state of charge. Their general conclusions indicated that diffusion processes play the dominant role in governing the impedance of NiCd cells. However, essentially no data exist on the impedance of NiCd cells at frequencies below 5 Hz, which is the range expected to be most important for processes involving diffusion and film growth.

5

Diffusion processes in both the alkaline electrolyte and in solid-state films at the electrodes are generally believed to be important in the operation of the NiCd cell. The overall reactions that take place at the positive and negative electrodes, respectively, can be represented approximately as

$$NiOOH + H_2O + e^- \xrightarrow[\text{charge}]{\text{discharge}} OH^- + Ni(OH)_2 \tag{1}$$

$$Cd + 2OH^- \xrightarrow[\text{charge}]{\text{discharge}} 2e^- + Cd(OH)_2 \tag{2}$$
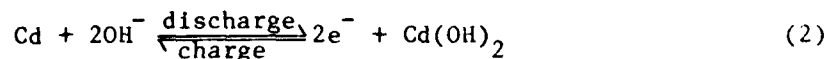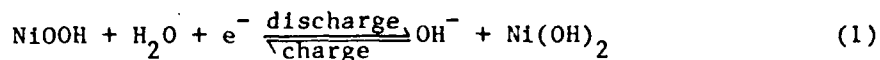
Because OH^- is produced and consumed at the electrodes during cell charge or discharge, diffusion of OH^- in the electrolyte must occur during the operation of the cell. In addition, film growth on the electrode surfaces or solid-state diffusion of species in the electrode active materials are processes that have been observed to occur in the NiCd electrode system. In the oxidation of the nickel electrode, MacArthur[6,7] identified solid-state proton diffusion from the oxidation site to the electrode electrolyte interface as a rate-limiting process. For planar cadmium electrodes, Armstrong and Edmondson[8] found that film growth is involved in the passivation of the cadmium electrode and that diffusion in this film controls reaction rates at the passivated electrodes. The problem of detecting and measuring these processes in the actual NiCd battery cell remains.

Detailed measurements of the impedance of a 10-Ah NiCd cell at frequencies ranging up to 200 kHz are presented in this report. The impedance in the lower frequency range is expected to provide information on the kinetics of the electrolyte and solid-state diffusion processes that are important in the

6

operation of the cell. The kinetics of such mass transport processes are determined over a range of operating currents, temperatures, and cell states-of-charge from the impedance measurements. Nickel cadmium cells are an important component of many secondary power systems. Impedance measurements over the wide frequency ranges reported here provide input data for the design and operation of such power systems.

II. EXPERIMENTAL

All measurements were for a 10-Ah sealed NiCd cell with electrodes of sintered-plate design. The cell (Serial No. Ll-137) was of prismatic design and was manufactured by General Electric. The impedance of this cell was measured at three states of charge while discharging the cell at various currents and temperatures. Before each discharge, the cell was brought to its fully charged state by charging for 16 hr at 1 A, after discharging it to less than 10 mV through a 1-ohm resistor. Discharge at constant current was begun immediately after charge termination. A Kepco BOP 36-5M power supply was used to charge and discharge the cell. For all experiments, the temperature of the cell was held constant in a temperature-controlled bath to $\pm 0.05°C$.

At frequencies below 10 Hz, a galvanostatic technique was used to measure the cell impedance. This technique consisted of the application of a current step to the cell in addition to the constant current discharge. The magnitude of this current step was 10% of the constant current discharging the cell, which gave a cell voltage response of less than 5 mV in all cases. The cell voltage was subtracted from a reference voltage, and this difference was amplified by a high input-impedance differential amplifier. The amplified voltage-response function was recorded, along with the cell current, on a dual-channel strip chart recorder with a full-scale response time of about 0.01 sec. These transient response measurements were made during each cell discharge at about 75, 50, and 25% of actual cell capacity (about 12.7 Ah). Measurements were done while the cell was undergoing constant current discharges of 4.5, 1.5, and 0.2 A at 25°C, and for 1.5-A discharges at 11 and

9

38°C. Measurements were also made after 24 hr on open circuit by measuring the voltage response to a 1-mA current step.

During discharge, the cell voltage exhibits a roughly linear decrease between about 20 and 80% of full charge. In this range, the cell voltage changed by less than 5 mV during each measurement, and a linear correction could be made to the data for the background decrease in cell voltage. The voltage-response function was digitized from the recorder output data, corrected for background, and converted to the frequency domain through a digital Laplace transformation following the general approach outlined by Pilla.[9] The Laplace transform of the current step is then computed, and the impedance is obtained as a function of frequency from the ratio of the transforms of voltage and current.

The cell impedance between 10 Hz and 200 kHz was measured with the use of a Hewlett-Packard 3575A gain-phase meter to monitor the gain and phase relationships between a sinusoidally alternating current and the voltage response of the cell to this current. In these experiments, the magnitude of the alternating current was chosen to provide a voltage response of less than 1 mV, and typically was 100 mA or less.

10

III. RESULTS

Typical data for the impedance of a NiCd cell are presented in the complex plane in Fig. 1. These data were obtained at 25°C while the cell was discharging at 1.5 A. The data below 10 Hz are from the galvanostatic transient technique and above 10 Hz from the alternating-current technique. The primary features are two relaxation processes in the upper (capacitive) quadrant and one major relaxation process in the lower (inductive) quadrant, as well as a smaller arc indicated in the inductive quadrant at several hundred hertz. These general features are common to all the experimental data. The inductive impedance (above 10 Hz) is relatively insensitive to cell state of charge and cell current and therefore is principally attributed to the self-inductance of the conductors and current collecting assemblies present at each electrode. This is consistent with previous results for the impedance of battery cells in this frequency range.[1,5,10] The inductance may be approximately represented as being equivalent to a parallel resistor inductor (R-L) combination in series with the remainder of the cell impedance. For the major inductive arc (Fig. 1), R is about 2 mohm and L is about 0.01 μH.

The impedance at frequencies below 10 Hz was found to be much more sensitive to cell current and state of charge. Two relaxation processes are observed in the upper quadrant of Fig. 1. The impedance of each of these processes appears to be characteristic of diffusion through a finite diffusion layer. At higher frequencies, the impedance is linear in the complex plane, with a slope of about 45 deg, whereas, at lower frequencies, the linear regime rolls over into a semicircle as diffusion becomes limited by the diffusion
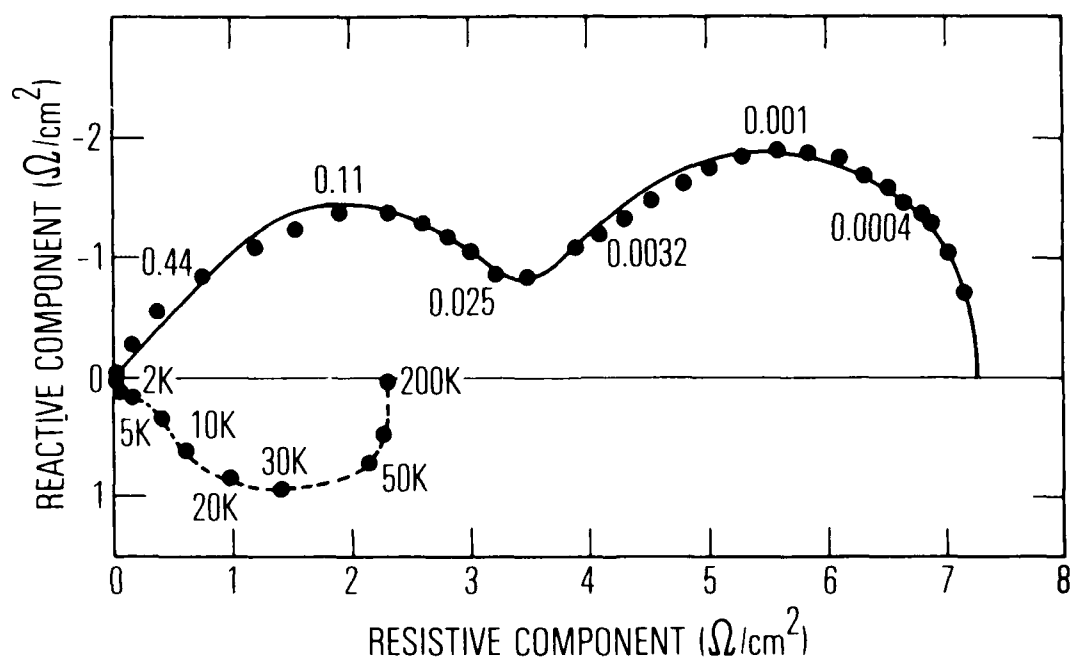
11

Fig. 1. Ten-Ampere Hour NiCd Cell Impedance. The frequencies, in hertz, are indicated by the numbers.

layer boundary. The data in Fig. 1 therefore indicate that two diffusion processes control the impedance of NiCd cells during discharge.

A more quantitative analysis of the impedance at low frequencies can be made by employing a model that describes the diffusion and charge transfer characteristics of the NiCd cell. In this analysis, the inductive impedance will not be considered because it is relatively insignificant at low frequencies, and because it appears to have little bearing on the electrochemical and mass transport processes occurring in the NiCd cell. The low-frequency impedance can be modeled by the equivalent circuit shown in Fig. 2. For each of the two processes, the diffusion impedance Z_D is coupled to the faradaic impedance, which is represented in Fig. 2 by the charge-transfer resistance R_C. The double-layer capacitance C_{DL} shunts the charge-transfer and diffusion-impedance contributions. The equivalent circuit of Fig. 2 is analogous to the Randles circuit,[11] except that the Warburg impedance of the Randles circuit is replaced by Z_D to model diffusion through a finite diffusion layer.

A number of assumptions are implicit in the model shown in Fig. 2. The charge-transfer impedance is represented by a resistance. This is likely to be a good approximation at low frequencies in the absence of slow intermediate adsorption processes. By associating each diffusion process with an interfacial charge-transfer step, we are also assuming that each electrode in the NiCd cell gives rise to one of the processes shown in Fig. 2. Because each electrode should contribute to the cell impedance, it seems reasonable to make this assumption initially. The diffusion model shown in Fig. 2 is most easily analyzed in terms of diffusion at planar electrode surfaces. However,
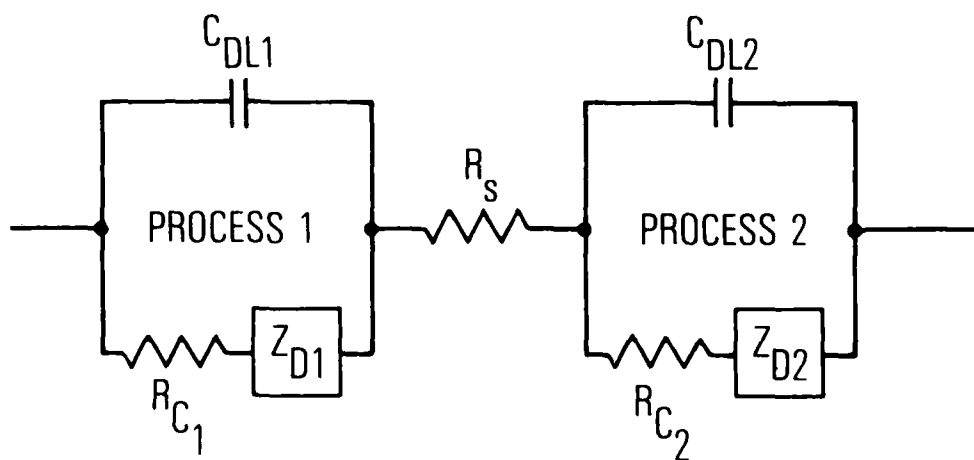
13

Fig. 2. Equivalent Circuit Used in Modeling the Low-Frequency Impedance of NiCd Cell.

the sintered electrodes in the NiCd cell have a porous structure, which will, in general, result in nonuniform current densities at the electrode surfaces or in their pore structure. In the first-order model presented below, the dispersive effects arising from nonuniform current densities are not considered. These effects can be modeled in terms of transmission line theory[12,13] and included in the model of cell impedance if necessary to adequately describe the experimental data.

The impedance of the equivalent circuit model of Fig. 2 is given by

$$Z = R_s + \sum_i (Y_i)^{-1} \qquad i = 1,2 \tag{3}$$

where Y_i is the admittance of process i,

$$Y_i = j\omega C_{DLi} + (R_{ci} + Z_{Di})^{-1} \tag{4}$$

The impedance Z_{Di} arising from diffusion through a finite diffusion layer is given by[14]

$$Z_{Di} = \sigma_i \omega^{-1/2}(1 - j) \tanh\left[\delta_i \left(\frac{j\omega}{D_i}\right)^{1/2}\right] \tag{5}$$

where σ_i is a Warburg coefficient, δ_i is the diffusion layer thickness, ω is the angular frequency, and D_i is the diffusion coefficient for the diffusing species. The relaxation time for a given diffusion process is

$$\tau \approx \frac{\delta^2}{D} \tag{6}$$

15

In the limit of low frequency, the diffusion impedance Z_D approaches the diffusion resistance, which is given by

$$R_o = \sigma\delta\left(\frac{2}{D}\right)^{1/2} \qquad (7)$$

The low-frequency impedance of a NiCd cell was found to fit Eq. (3) quite well in the operating range of the cell under all conditions for which measurements were made. A nonlinear fitting routine[*] was used to simultaneously fit the resistive and reactive components of the cell impedance to Eq. (3). A typical fit is indicated for the data in Fig. 1 by the solid line. Data at frequencies above 100 Hz were not considered in fitting the results since the higher frequency inductive components were not included in the model for the cell impedance. Furthermore, the data were fitted to Eq. (3) under the assumption that R_c was negligible relative to Z_D, that is, the cell impedance was predominantly controlled by diffusion rather than by charge transfer. For frequencies below 10 Hz, this appears to be a good approximation, although differences between the modeled and experimental data at higher frequencies, particularly at the highest currents where Z_D was relatively small, may arise from neglecting the charge-transfer resistance.

The parameters that describe the diffusion impedance characteristics for each of the processes in Fig. 2 are C_{DL}, σ, and τ. The results of

---

[*]The fitting routine used was obtained from: H. J. Wertz, "GAUSAUS-Nonlinear Least Squares Fitting and Function Minimization," Mathematics and Computation Center, The Aerospace Corporation, El Segundo, California (1968) (unpublished).

measurements at various cell discharge currents are given in Figs. 3 and 4 for
σ and τ, respectively, for the two processes at 25°C and roughly at 50% state
of charge. Each point is an average of three measurements, with the standard
deviations represented by the error bars. The higher frequency process is
designated process 1; the lower frequency one, process 2. All impedances,
current densities, and capacitances are given in terms of the geometric areas
of the positive and negative electrode plates, which are 840 and 924 cm^2 for
the positive and negative, respectively. For simplicity, a geometric area of
1000 cm^2 is assumed for both processes, because it is not clear at which
electrode each process occurs. Note that the actual active electrochemical
areas of sintered-plate electrodes may be more than an order of magnitude
greater than the geometric plate areas and will depend on both active material
and sinter structures.

The capacitance C_{DL} for each of the two processes presented in Fig. 2
will generally include any pseudocapacitance arising from absorbed surface
species, in addition to the capacitance of the interfacial double layer. For
process 1, the measured capacitance was typically found to be in the range 10
to 100 $\mu F/cm^2$, and, for process 2, the capacitance ranged from 100 to 20,000
$\mu F/cm^2$. Within these ranges, the capacitance was sufficiently variable that
no systematic dependence on temperature, current, or state of charge could be
distinguished. The large variability in these capacitances is because the
equivalent capacitance arising from diffusion ranges up to several farads per
square centimeter in the frequency range over which the data were fitted.
Because the value of C_{DL} is only a very small part of the overall equivalent
capacitance, the precision of the measurements is insufficient to provide
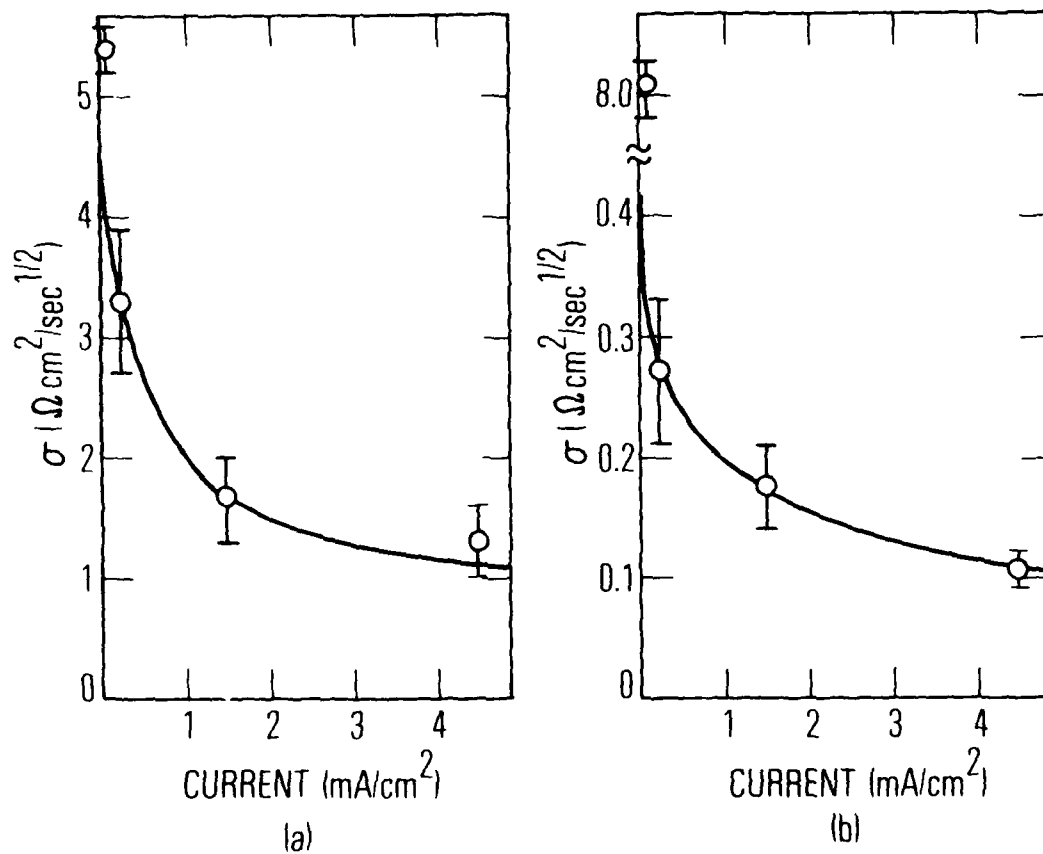reproducible values for C_{DL}.

Fig. 3. Warburg Coefficient as Function of Current for NiCd Cell. (a) For
higher frequency diffusion process. (b) For lower frequency process.
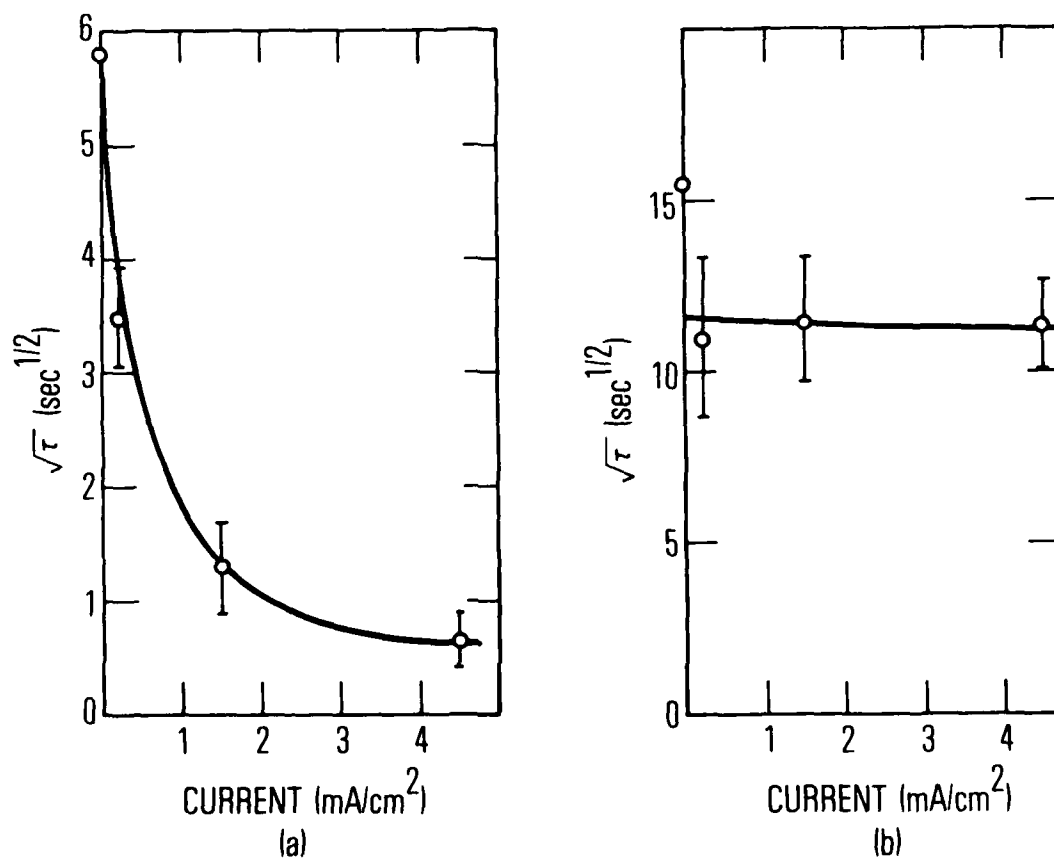
Fig. 4. Square Root of Relaxation Time for Diffusion Processes Observed for NiCd Cell. (a) For higher frequency process. (b) For lower frequency process.

19

The diffusion resistance, defined by Eq. (7) for each of the two observed processes, was found to exhibit some dependence on the state of charge of the cell. The dependence of R_o on cell state of charge is indicated in Fig. 5 at various discharge currents for a cell temperature of 25°C. The solid lines in Fig. 5 are only meant to show the trends in the data. The diffusion resistance exhibited only a very slight dependence on temperature over the range 12 to 38°C. The diffusion resistance for process 1 increased about 20%, and that for process 2 decreased about 30% over this temperature range. Although these changes are greater than the scatter in the data, they were not great enough to permit a detailed analysis.
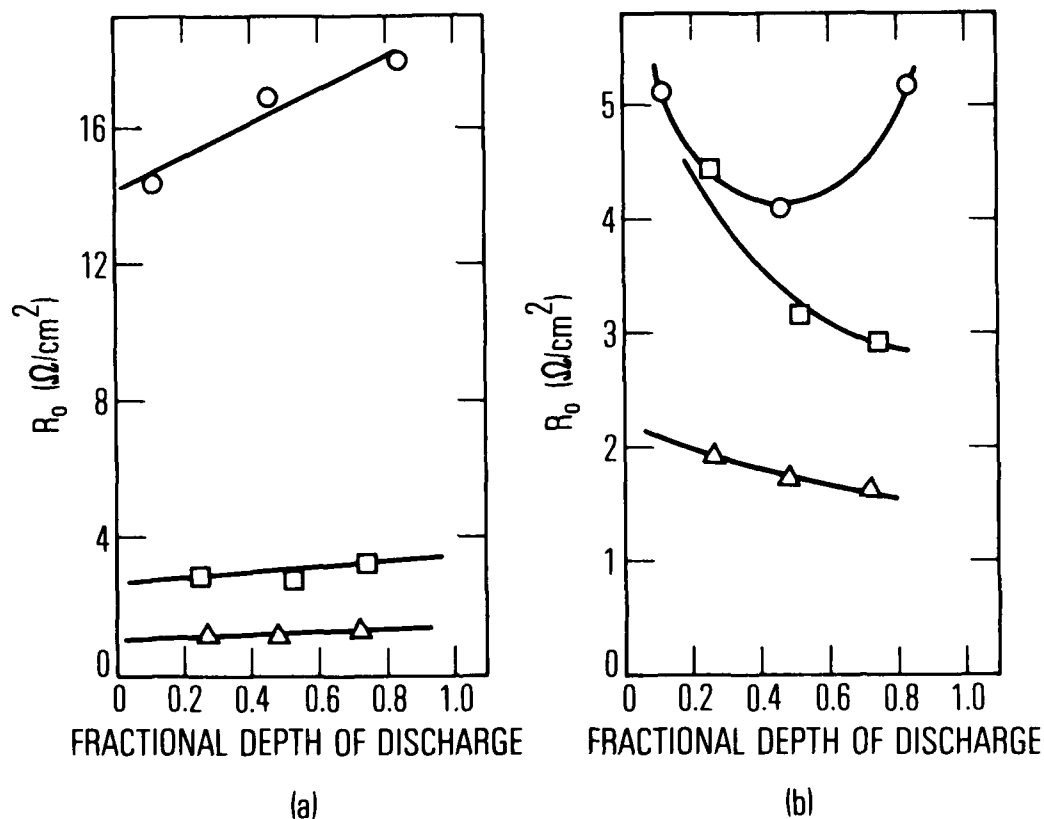
Fig. 5. Diffusion Resistance of NiCd Cell at 25°C as Function of Depth of
Cell Discharge at Various Discharge Currents. (a) For process 1.
(b) For process 2. The discharge currents are 0.2 A (circles), 1.5 A
(squares), and 4.5 A (triangles).

IV. DISCUSSION

The assignment of the two capacitive relaxation processes in the low-frequency impedance data of Fig. 1 to diffusion-controlled processes is suggested by the frequency dispersion associated with each peak in Fig. 1. The simple first-order diffusion model (Fig. 2) provided a good fit to the data. However, a good fit can also be obtained with the use of a model that assumes that charge-transfer reactions control the impedance and that an additional capacitive dispersion arises from nonuniform current distribution in the porous electrodes. If charge transfer were controlling the impedance in this manner, double layer and pseudocapacitances of approximately 0.5 and 40 F/cm^2 would be necessary for processes 1 and 2, respectively, to adequately fit the experimental data. These capacitances seemed unreasonably large, so the model shown in Fig. 2 was adopted. This model assumes a uniform current distribution within the double layer, where the impedance is controlled by the diffusion of species to the sites at which charge transfer occurs. The model fits the data quite well, indicating that the effects of nonuniform current distribution are not great for the two observed processes. Any significant contribution to the impedance from nonuniform current distributions would result in an impedance that rises with a slope of less than 45 deg[13] in the complex plane of Fig. 1. Over the range of cell operating conditions examined in this study, no significant additional frequency dispersion of this kind was observed.

For the model described by Fig. 2, the Warburg coefficient σ can be represented by[14]

$$\sigma = \frac{RT}{n^2 F^2 c \sqrt{2D}} \tag{8}$$

where c is the concentration of diffusing species, and D is the diffusion coefficient. As indicated in Fig. 3, σ decreases as current is increased for both processes. Eq. (8) indicates that this might be because the concentration of diffusing species increases as current is increased, which is consistent with these species being either produced or consumed in the charge-transfer reactions. The dependence of relaxation time on current (Fig. 4a) can be qualitatively understood from Eq. (6). As current increases, the diffusion layer thickness δ decreases, resulting in a time constant that decreases as is observed for process 1. However, for process 2 (Fig. 4b), the diffusional relaxation time does not decrease significantly with increasing current. This suggests that, in the typical operating current range of the NiCd cell, the diffusion-layer thickness and the diffusion coefficient for process 2 both change with current such that the relaxation time has little current dependence. Such a situation could result from solid-state diffusion in a surface film for which the morphology of the film depends on the current. It is, in fact, expected that the structure and morphology of a surface film will depend on the current density at which the film is formed[15,16] and that the coefficient for diffusion in this film will depend on the dynamic conditions under which the film was formed.

From Eq. (8), we estimate the value of $c \sqrt{D} \approx 1 \times 10^{-7}$ mole cm^{-2} $sec^{-1/2}$ for process 1 and $c \sqrt{D} \approx 1 \times 10^{-6}$ mole cm^{-2} $sec^{-1/2}$ for process 2. In measurements of the impedance of flat cadmium electrodes, Armstrong and Edmondson[8] have obtained values of about 2×10^{-10} mole cm^{-2} $sec^{-1/2}$ for

24

$c \sqrt{D}$ for the interfacial diffusion of intermediate cadmiate species in 10 M KOH electrolyte. However, note that this value is in terms of the electrochemically active area, which, in the case of sintered plates, is much greater than the geometric area that we used in calculating $c \sqrt{D}$. For the sintered nickel electrode, MacArthur[7] measured $c \sqrt{D} = 1.6 \times 10^{-7}$ mole cm^{-1} sec$^{-1/2}$ for diffusion of protons in the nickel hydroxide lattice during discharge in alkaline electrolyte. It is likely that processes 1 and 2 correspond to cadmiate diffusion at the cadmium electrode and solid-state proton diffusion at the nickel electrode. Although this is reasonably consistent with the known electrochemistry of the nickel and cadmium electrodes, further measurements employing a reference electrode in the cell will be necessary to definitively assign these processes.

The diffusion resistance R_0 has a systematic dependence on the depth to which the cell is discharged, as indicated in Fig. 5 at various discharge currents. From Eqs. (7) and (8),

$$R_0 = \frac{RT\delta}{n^2 F^2 cD} \tag{9}$$

For process 1, R_0 increases as the cell is discharged. This is to be expected because the diffusion coefficient should decrease as films build up during discharge, and the active surface area should decrease as the cell is discharged. However, process 2 exhibits a more complicated behavior (Fig. 5b) revealing a generally decreasing diffusion resistance as discharge progresses. It is possible that this behavior results from the selective discharge of the γ and β structures of $NiOOH$.[17] In any case, it is likely that a more

25

detailed model that considers the various forms of NiOOH and their nonstoi-chiometric properties will be required to fully account for the impedance properties of the nickel electrode.

SYMBOLS

c concentration of diffusing species, moles/cm^3

C_{DLi} double layer capacitance for process i, F/cm^2

D_i diffusion coefficient for diffusing species i, cm^2/sec

F Faraday's constant, 96,487 C/equiv

j $\sqrt{-1}$

L high-frequency cell inductance, μH

n number of electrons transferred in an electrode reaction

R high-frequency cell resistance, ohms

R_{ci} charge-transfer resistance for process i, ohms/cm^2

R_s electrolyte resistance, ohms

R_o diffusion resistance, ohms/cm^2

RT gas constant multiplied by the absolute temperature, joules/mole

Y_i admittance of process i, cm^2/ohm

Z battery cell impedance, ohms

Z_{Di} diffusion impedance for process i, ohms/cm^2

δ_i diffusion layer thickness for process i, cm

σ_i Warburg coefficient for process i, ohm cm^2/sec$^{-1/2}$

τ diffusional relaxation time, sec

ω angular frequency, rad/sec

27

REFERENCES

1. R. J. Brodd and H. J. DeWane, *J. Electrochem. Soc.*, 110, 1091 (1963).

2. M. Keddam, Z. Stoynov, and H. Takenouti, *J. Appl. Electrochem.*, 7, 539 (1977).

3. P. Bauer, *Batteries for Space Power Systems*, SP-172, National Aeronautics and Space Administration, 1968, pp. 89-95.

4. M. Lurie, H. N. Seiger, and R. C. Shair, *State of Charge Indicators for Nickel Cadmium Batteries*, ASD-TDR-63-191, Gulton Industries, Metuchen, N.J. (1963).

5. S. Sathyanarayana, S. Venugopalan, and M. L. Gopikanth, *J. Appl. Electrochem.*, 9, 125 (1979).

6. D. M. MacArthur, *J. Electrochem. Soc.*, 117, 422 (1970).

7. D. M. MacArthur, *J. Electrochem. Soc.*, 117, 729 (1970).

8. R. D. Armstrong and K. Edmondson, *Electroanal. Chem. Interfacial Electrochem.*, 53, 371 (1974).

9. A. A. Pilla, *J. Electrochem. Soc.*, 117, 467 (1970).

10. M. L. Gopikanth and S. Sathyanarayana, *J. Appl. Electrochem.*, 9, 369 (1979).

11. J. E. B. Randles, *Disc. Faraday Soc.*, 1, 11 (1947).

12. R. DeLevie, *Electrochim. Acta*, 8, 751 (1963).

13. R. DeLevie, *Electrochim. Acta*, 9, 1231 (1964).

14. P. Drossbach and J. Schultz, *Electrochim. Acta*, 9, 1391 (1964).

15. Y. Okinaka and C. Whitehurst, *J. Electrochem. Soc.*, 117, 583 (1970).

16. D. Chua and R. J. Diefendorf, *Proceedings of the 25th Power Sources Symposium*, (1972) pp. 52-55.

17. H. Bode, K. Dehmelt, and J. Witte, *Electrochim. Acta*, 11, 1079 (1966).

LABORATORY OPERATIONS

The Laboratory Operations of The Aerospace Corporation is conducting experimental and theoretical investigations necessary for the evaluation and application of scientific advances to new military concepts and systems. Versatility and flexibility have been developed to a high degree by the laboratory personnel in dealing with the many problems encountered in the nation's rapidly developing space and missile systems. Expertise in the latest scientific developments is vital to the accomplishment of tasks related to these problems. The laboratories that contribute to this research are:

Aerophysics Laboratory: Launch and reentry aerodynamics, heat transfer, reentry physics, chemical kinetics, structural mechanics, flight dynamics, atmospheric pollution, and high-power gas lasers.

Chemistry and Physics Laboratory: Atmospheric reactions and atmospheric optics, chemical reactions in polluted atmospheres, chemical reactions of excited species in rocket plumes, chemical thermodynamics, plasma and laser-induced reactions, laser chemistry, propulsion chemistry, space vacuum and radiation effects on materials, lubrication and surface phenomena, photosensitive materials and sensors, high precision laser ranging, and the application of physics and chemistry to problems of law enforcement and biomedicine.

Electronics Research Laboratory: Electromagnetic theory, devices, and propagation phenomena, including plasma electromagnetics; quantum electronics, lasers, and electro-optics; communication sciences, applied electronics, semiconducting, superconducting, and crystal device physics, optical and acoustical imaging; atmospheric pollution; millimeter wave and far-infrared technology.

Materials Sciences Laboratory: Development of new materials; metal matrix composites and new forms of carbon; test and evaluation of graphite and ceramics in reentry; spacecraft materials and electronic components in nuclear weapons environment; application of fracture mechanics to stress corrosion and fatigue-induced fractures in structural metals.

Space Sciences Laboratory: Atmospheric and ionospheric physics, radiation from the atmosphere, density and composition of the atmosphere, aurorae and airglow; magnetospheric physics, cosmic rays, generation and propagation of plasma waves in the magnetosphere; solar physics, studies of solar magnetic fields; space astronomy, x-ray astronomy; the effects of nuclear explosions, magnetic storms, and solar activity on the earth's atmosphere, ionosphere, and magnetosphere; the effects of optical, electromagnetic, and particulate radiations in space on space systems.

THE AEROSPACE CORPORATION
El Segundo, California